COMMUNICATIONS IN SCIENCE AND TECHNOLOGY
Homepage: cst.kipmi.or.id

High-performance eco-friendly Ni-Cu/bamboo activated carbon catalysts for oxidative desulfurization of high-concentration DBT

St. Haerani [a], Wega Trisunaryanti [a,*], Triyono[a], Imam Santoso[b], Jason Purbonegoro [a], Wangsa [a]

[a]*Department of Chemistry, Gadjah Mada University, Yogyakarta, 55281, Indonesia*
[b]*Department of Physics, Gadjah Mada University, Yogyakarta, 55281, Indonesia*

Article history:
Received: 3 July 2025 / Received in revised form: 25 October 2025 / Accepted: 28 October 2025

Abstract

This study investigated how the metal impregnation method affects the oxidative desulfurization (ODS) of dibenzothiophene (DBT) using H_2O_2 over Ni–Cu catalysts supported on bamboo-derived activated carbon. Catalysts with 1% and 2% Ni–Cu were prepared via simultaneous impregnation, while the effect of sequence was evaluated by comparing simultaneous and sequential impregnation (2%Ni-2%Cu/AC and 2%Cu-2%Ni/AC). The 2%Ni-2%Cu/AC catalyst was identified as the best catalyst, with a surface area of 802.36 m²/g, average pore diameter of 2.4761 nm, and total acidity of 3.1239 mmol/g. This catalyst achieved the highest DBT reduction of 90.81% under optimal conditions (0.2 g catalyst weight, 60 minutes, 40 °C, and 0.66 mL H_2O_2), confirming that the sequential impregnation route significantly enhances catalytic performance. In conclusion, the impregnation sequence in designing highly efficient desulfurization catalysts is important due to spray impregnation resulting in higher surface area, acidity, and catalytic activity compared to the simultaneous impregnation method.

Keywords: Activated carbon; dibenzothiophene; impregnation sequence; nickel copper; oxidative desulfurization

1. Introduction

The emission of sulfur oxides (SO_x) generated from the combustion of fuel containing sulfur compounds can lead to air pollution and acid rain. In addition, they have corrosive effects that can reduce the engine life and also deactivate catalysts during fuel oil processing [1,2]. The maximum sulfur content standard in fuel oil for transportation purposes in many countries is 10-15 ppm [3]. Therefore, an effective and efficient desulfurization method is required to produce low-sulfur fuel oil. Hydrodesulfurization (HDS) is widely used industrially but is inefficient for removing refractory aromatic sulfur compounds like thiophene, BT, and DBT due to their steric stability [4–6]. It also requires high temperature, high pressure, and hydrogen, making the process costly [7,8].

Oxidative desulfurization (ODS) is considered superior to other methods because it is efficient in removing aromatic sulfur compounds, operates at low temperatures and pressures, and has high desulfurization efficiency without the need of hydrogen [2]. According to Jia et al. [9], sulfur compounds that are difficult to remove in HDS are highly reactive in ODS. The ODS process involves two stages: first, sulfur compounds are oxidized into more polar sulfoxides and sulfones using an oxidant and catalyst; then, the oxidized products are separated via polar solvent extraction [10]. Catalyst design is crucial for achieving high ODS efficiency.

Transition metal catalysts provide abundant active sites with high activity, selectivity, and stability. Although noble metals like Pt and Au are effective for ODS [11–13], their high cost limits use. More affordable metals such as Ni and Cu are widely applied, with unpaired electrons and empty p orbitals that act as acid sites to facilitate H_2O_2 decomposition [14,15]. In the ODS process, Yaseen et al. [14] demonstrated that Ni and Cu supported on activated carbon achieved DBT conversions of 93% and 90%, respectively. Compared to monometallic catalyst, bimetallic catalyst can outperform because two metals can create a synergy resulting in higher catalytic activity [16].

The use of metal catalysts requires a catalytic support that not only facilitates the dispersion of active metals but also enhances catalytic activity [17,18]. Activated carbon has high porosity, surface area, and functional groups on its surface and is readily available [19,20]. Activated carbon can be produced from lignocellulosic biomass such as bamboo, which is widely used in construction and crafts, generating large amounts of waste suitable for conversion. [21]. Bamboo is estimated to contain 45.2% cellulose, 10.81% hemicellulose, and 28.35% lignin, with low inorganic content [22], making it a suitable raw material for producing activated carbon.

The metal loading method strongly affects particle dispersion and catalyst performance. Excess metal can disrupt metal-support interactions [23,24], so optimizing both the amount and sequence of Ni and Cu addition on activated carbon is essential to achieve superior catalytic properties. The

* Corresponding author. Tel.: +62-811-282-985; fax +62-274-545-188
Email: wegats@ugm.ac.id
https://doi.org/10.21924/cst.10.2.2025.1702

impregnation method affects the catalytic activity where it can affect it surface area as reported by Osakoo et al. [25] that stated sequential impregnation improved catalytic activity for Fischer–Tropsch synthesis due to higher surface area than simultaneous impregnation.

This research investigates how metal impregnation method and sequence influence the oxidative desulfurization (ODS) of dibenzothiophene (DBT) using H_2O_2 over Ni–Cu bimetallic catalysts supported on bamboo-waste-derived activated carbon. The catalysts were designed as eco-friendly systems and tested under a high-sulfur feed (1200 ppm DBT), a significantly harsher and more realistic condition than typically reported in the literature. Compared to other metal impregnation, spray impregnation was used for the synthesis that uses less solution, which led to less metal loss in the solution during the synthesis process, especially in sequential bimetallic impregnation that involved two different solutions during synthesis. The effects of metal content and preparation order on catalyst properties and activity were also studied. The catalyst was tested in the ODS-DBT process with H_2O_2 as an oxidant and acetonitrile as an extractant, examining the impact of dosage, time, temperature, and O/S ratio on DBT removal.

2. Materials and Methods

2.1. Materials

The material used in this study were Petung bambu (*Dendrocalamus asper)* waste collected from Grosir Bambu Petung Mulia Jaya, Ltd. (Yogyakarta, Indonesia); Phosphoric acid (H_3PO_4) (85%); Nickel nitrate hexahydrate p.a. ($Ni(NO_3)_2.6H_2O$); Copper nitrate trihydrate p.a. ($Cu(NO_3)_2.3H_2O$); Dibenzothiophene ($C_{12}H_8S$ 99% purity, Merck); n-hexane (C_6H_{14}); Hydrogen peroxide (H_2O_2 30%); Acetonitrile (CH_3CN); Nitrogen (N_2) gases were supplied by Samator Gas Industri, Ltd. (Yogyakarta, Indonesia).

2.2. Preparation of activated carbon from bamboo waste

Petung bamboo waste was collected from Grosir Bambu Petung Mulia Jaya, Yogyakarta. It was cleaned and sun dried in 20 hours and dried using oven at 110 °C for 24 hours. The dried bamboo waste was crushed and sieved to a size 0.2-0.5 cm. Modified from a study by Ismail et al. [26], The sieved bamboo was pre-treated by soaking in the H_3PO_4 (85%) with a ratio of 1:1 (w/v) for 24 hours at room temperature. The precursor was then carbonized in a furnace at 600 °C for 4 hours under N_2 atmosphere with the flow rate of 20 mL/min. After carbonization, samples were cooled, washed with deionized water until pH value of the filtrate becomes the same as deionized water, i.e. pH 5-6. Finally, the sample was dried using oven at 100 °C for 24 hours and then sieved using a 200-mesh sieve. The activated carbon namely AC.

2.3. Preparation of bimetal catalysts

The varied Ni-Cu/AC catalysts were prepared by using spray impregnation which was modified from a study by Triyono et al. [27]. The AC was impregnated with the aqueous solution of $Ni(NO_3)_2.6H_2O$ dan $Cu(NO_3)_2.3H_2O$ to obtain Ni and Cu precursor. The first one, the catalysts were prepared by co-impregnation method with the concentration of each metal varied by 1% and 2%. Both Ni and Cu precursors were dissolved in deionized water and spraying to AC. Then dried at 100 °C for 18 h and calcination at 500 °C for 4 h under N_2 gas flow 20 mL/min. This made the 1%Ni1%Cu/AC and 2% Ni2%Cu/AC catalysts.

In the sequential impregnation method, it was carried out with each metal loading 2%. The Ni solution was first loaded onto AC by spray impregnation and dried at 100 °C for 18 h. The obtained sample was subsequently impregnated with the Cu solution and dried again at 100 °C for 18 h, finally calcined at 500 °C for 4 h under N_2 gas flow 20 mL/min. It is obtained the 2%Ni-2%Cu/AC. The last one was prepared by first Cu impregnation and then Ni, the preparation process is same to previous method except exchanging the additional order to the Ni and Cu precursors and this is obtained the 2%Cu-2%Ni/AC catalyst.

2.4. Catalysts characterization

The varied catalysts were analyzed by FTIR (Fourier Transform Infra-Red, Shimadzu Prestige-21) to observe their functional groups in the range 4000 to 400 cm^{-1} with the KBr technique which is a standard technique in FTIR characterization. Despite the presence of metallic Ni and Cu species, the catalysts were finely ground and homogeneously mixed with KBr to ensure adequate IR transmittance. For metal content analysis, X-Ray fluorescence (XRF, RIGAKU NEX CGII) was used. The crystallinity and diffraction patterns of the catalysts were characterized using XRD (Bruker Phase D2). SEM Mapping elements (SEM, JEOL JSM-6510) were used to analyze the catalysts morphology, along with EDX to evaluate the amounts of metal contained. The catalysts porosity was examined by nitrogen adsorption-desorption isotherms at 77K using SAA (Quantachrome NovaWin Series), then the data were analyzed by BET and BJH methods. The catalyst acidity was determined by NH_3-TPD (Chemisorb 2750 Micromeritics).

2.5. Catalytic activity test in ODS-DBT

The model fuel was prepared by dissolving DBT in n-hexane at a concentration of 1200 ppm. Using the method from previous study [7], the ODS process was carried out in a 250 mL three neck round bottom flask, equipped with a condenser fitted with magnetic stirrer and immersed in an oil bath controlled by thermometer. The catalytic activity of all catalyst variants was investigated in a standard reaction. A mixture of 20 mL model oil and 20 mL acetonitrile (extractant) was added to the flask and heated under vigorous stirring (600 rpm). After the temperature reached 60 °C, 0.15 g of catalyst and 0.13 mL of H_2O_2 (equivalent to 15wt% active H_2O_2 based on the total

mass of catalyst and oxidant, using a 30wt% H_2O_2 solution) were added to initiate the reaction, which proceeded for 60 minutes. After the reaction, the catalyst was separated from the mixture using centrifuge and two phases of the solvent-model fuel mixture are then decanted in separating funnel for 15 minutes to reach polar solvent and model fuel phases. The fuel phase was diluted then the absorbance was measured at 286 using UV-Vis spectrophotometer. The calibration curve method was used to determine the concentration of DBT in the fuel phase. A series of standard solutions were made by diluting a 1200 ppm DBT solution into 3, 6, 9, 12, and 15 ppm. The decrease in DBT concentration can be calculated using the following equation, where C_0 and C_t are the initial and final concentrations of DBT, respectively.

$$\text{DBT removal (\%)} = \frac{C_0 - C_t}{C_0} \times 100\% \quad (1)$$

Using the best catalyst, the effects of catalyst loading, temperature, reaction time, and the hydrogen peroxide-to-sulfur ratio were investigated by conducting the ODS reaction under various conditions. Catalyst loading ranged from 0.05 to 0.25 g, reaction time from 20 to 120 minutes, and temperature from 30 to 70 °C. The volume of hydrogen peroxide used (relative to sulfur) varied from 0.066 to 0.66 mL.

2.6. Reusability test

Some experiments were conducted to inspect the reusability of the catalyst. In these experiments, using the optimal conditions, after the initial use of catalyst, the catalyst was recovered from the reaction solution by centrifugation. Then the catalyst was washed with acetonitrile and heated up to 100 ˚C until its weight was constant to remove residual solvent. The next run was then performed in the reactor with fresh model fuel, H_2O_2 and acetonitrile.

3. Results and Discussion

3.1. Catalysts characterization

The FTIR spectra was used to confirm the presence of functional groups in the sample as seen in Fig. 1. Bamboo waste spectra in the Fig. 1. show a broad and strong absorption at 3415 cm^{-1} which refer to O-H stretching vibration due to the presence of water, alcohols, phenols and carboxylic acid. A strong absorption at 2918 cm^{-1} is caused by aliphatic C-H stretching vibration. C=O stretching vibration of carbonyl group were detected at an absorption peak of 1735 cm^{-1}, C=C double bond from aromatic skeleton vibration of lignin at 1604 cm^{-1}, and C-O stretching vibration at 1050 cm^{-1}, which is found in cellulose, hemicellulose, and lignin [28]. The AC shows a decrease in O-H stretching vibration absorption compared to bamboo waste. Other absorption peaks also disappear in the AC. This is indicated that the carbonization process release water and volatile compounds from the bamboo waste. The absorption peak at 1560 cm^{-1} represents C=C stretching vibration of aromatic rings, which is the characteristic functional group of activated carbon. The broad absorption peak in the range of 1000-1300 cm^{-1} is indicate the P-O, C-O stretching vibration from C-O-P bonds or P-OOH, from the activation process of bamboo waste using phosphoric acid [29,30]. The FTIR spectra of Ni and Cu catalysts impregnated on AC in Fig. 2 show similar absorption peak with AC. This shows that the metal impregnation process does not significantly affect the presence of functional groups on the AC [23].

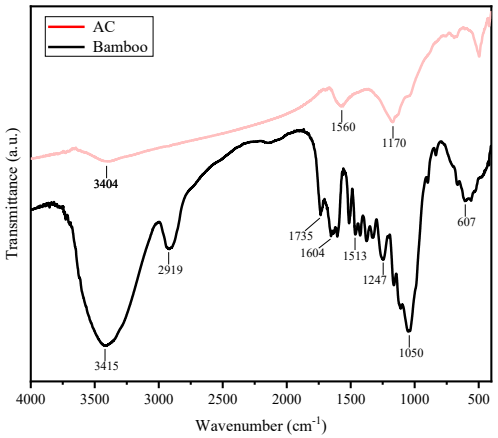

Fig. 1. FTIR spectra of bamboo and AC

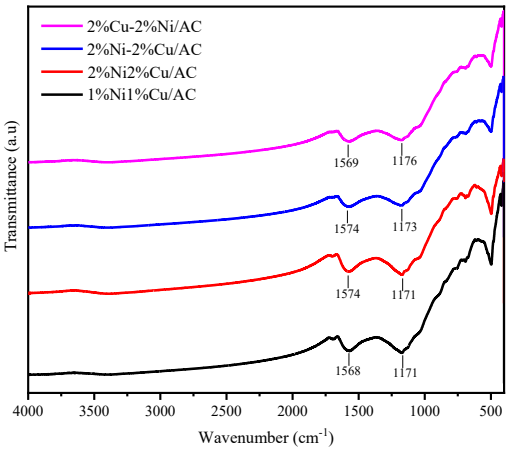

Fig. 2. FTIR spectra of synthesized catalysts

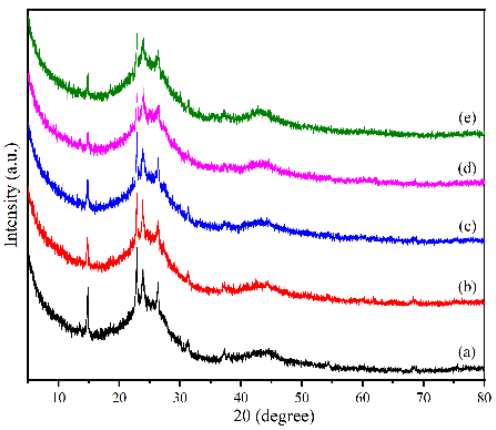

Fig. 3. XRD patterns of (a) AC, (b) 1%Ni1%Cu/AC, (c) 2%Ni2%Cu/AC, (d) 2%Ni-2%Cu/AC, and (e) 2%Cu-2%Ni/AC

The diffraction patterns of all catalysts are presented in Fig. 2. It showed two weak and broad peaks around 2θ= 21-27˚ and 2θ= 43-47˚ which were identified as the (002) and (100) crystal planes of graphite with an amorphous phase [7,29]. After impregnating with bimetallic Ni and Cu, the diffraction patterns did not show significant additional peaks for Ni and Cu metals. The XRD patterns are dominated by the broad turbostratic carbon peak of the activated carbon support, and no distinct reflections of Ni or Cu are observed where the expected peaks of NiO is around 2θ= 37-43˚ with (111) crystal planes and CuO around 35-38˚ with (111) crystal planes [31,32]. This behavior may be caused by low metal loadings on carbon supports, as highly dispersed or nanocrystalline NiO/CuO species (<5–10 nm) produce broad, low-intensity peaks that are readily masked by the strong amorphous carbon background [33]. For example, Zeng et al. [31] similarly observed that NiO peaks in the 2θ = 37–43° region were suppressed by the carbon support. Although phase-matching software did not confirm NiO or CuO due to the low signal intensity, the presence of Ni and Cu on the activated carbon is confirmed by the elemental analysis results shown in Fig. 5 and Table 1.

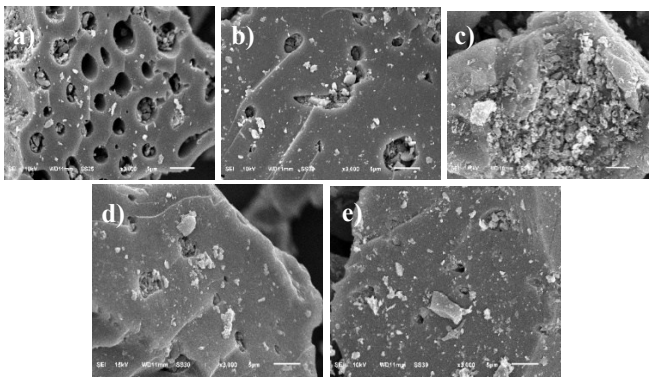

Fig. 4. SEM images of (a) AC, (b) 1%Ni1%Cu/AC, (c) 2%Ni2%Cu/AC, (d) 2%Ni-2%Cu/AC, and (e) 2%Cu-2%Ni/AC

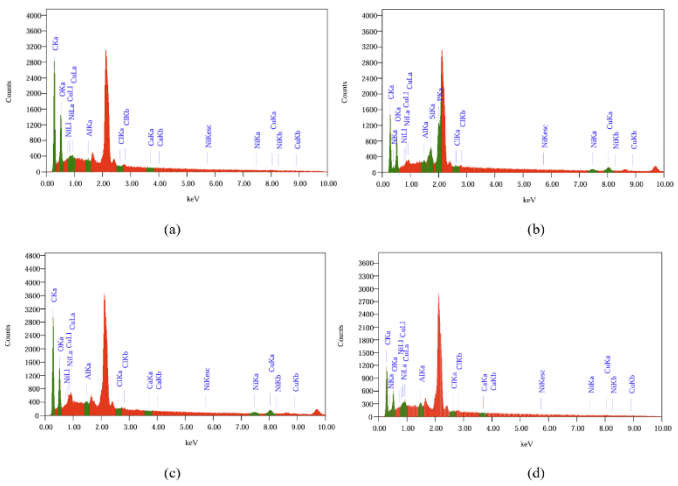

Fig. 5. Metal content analysis of (a) 1%Ni1%Cu/AC, (b) 2%Ni2%Cu/AC, (c) 2%Ni-2%Cu/AC, and (d) 2%Cu-2%Ni/AC using EDX

SEM-EDX analysis was applied to analyze the morphology of the materials and further investigation of the content and dispersion of metals, Energy Dispersive X-ray Spectroscopy (EDX) and X-Ray fluorescence (XRF) were used for elemental analysis of the catalysts, as shown in Fig. 5 and Table 1. The detection of Ni and Cu metals via XRF was caused by bamboo's natural absorption and accumulation of transition metals, such as Ni and Cu, from the growth environment. As a result, trace levels of these metals are commonly retained in bamboo-derived activated carbon [34]. The 2%Ni2%Cu/AC catalyst where Ni and Cu metals are impregnated simultaneously, there are aggregates suspected to be metal particles on the AC surface that appear to have agglomerated so that they are not evenly distributed while the 2%Ni-2%Cu/AC and 2%Cu-2%Ni/AC catalysts where Ni and Cu metals are impregnated sequentially, the metals are distributed more evenly compared to 2%Ni2%Cu/AC as shown in Table 2. The AC pores are also blocked but not comparable to the pore block in the catalyst with simultaneous impregnation as seen in Fig 4.

Both EDX and XRF report higher apparent metal wt% than the nominal 2wt%, which is attributed to partial mass loss of the activated carbon support during calcination, effectively enriching the metal fraction as reported from studies by a Montaño et al. and Kurnia et al. where they reported mass loss on activated carbon after calcination [35,36].

Table 1. Metal content of AC and synthesized catalysts using XRF and EDX

Catalysts	Ni content (wt%)		Cu content (wt%)	
	XRF	EDX	XRF	EDX
AC	0.40	-	0.11	-
1%Ni1%Cu/AC	2.10	4.39	2.11	12.99
2%Ni2%Cu/AC	4.77	4.77	17.56	17.56
2%Ni-2%Cu/AC	3.78	3.78	13.83	13.83
2%Cu-2%Ni/AC	12.50	12.50	4.55	4.55

Table 2. Textural properties and acidity of AC and synthesized catalysts

Catalysts	S_{BET} (m^2/g)	V_P (cm^3/g)	Acidity (mmol/g)
AC	751.93	0.57	0.62
1%Ni1%Cu/AC	757.23	0.56	0.84
2%Ni2%Cu/AC	740.19	0.58	0.93
2%Ni-2%Cu/AC	802.36	0.61	3.12
2%Cu-2%Ni/AC	835.71	0.64	2.68

The impregnation of Ni and Cu bimetals on the AC surface resulted in an increase in surface area for most of the catalysts as seen in Table 2, except for 2%Ni2%Cu/AC. Catalysts prepared using sequential impregnation have a larger surface area compared to simultaneous impregnation. The decrease in surface area observed in the 2%Ni2%Cu/AC catalyst is likely due to Ni and Cu metals competing to adhere in the AC surface at the same time, causing both metals to interact more with themselves rather than with the support surface. As a result, the metal particles may aggregate, forming clusters or lumps, and block the available pores as seen in Fig. 4(c) and study by Aryee et al. stated that the decrease of surface

area was likely by pore blockage by the metal nanoparticles [37]. In contrast, the 2%Ni-2%Cu/AC and 2%Cu-2%Ni/AC catalysts prepared with sequential impregnation allow the metals to disperse more evenly causing the increase of surface area. The increase of surface area also may be caused by surface roughening where the metal crystallites formed dispersedly as seen in Fig. 4(d-e) and a study by Neisan et al. that showed metal deposition onto activated carbon increased its surface area due to the metal nanoparticle created additional active sites and surface roughness [38]. The 2%Cu-2%Ni/AC catalyst had higher surface area likely due to the Cu metal having less strong interacting with Ni metal that led to less pore blocking during first impregnation [39] while Ni metal for first impregnation caused higher acidity due to strong interaction with oxygen functional groups [40].

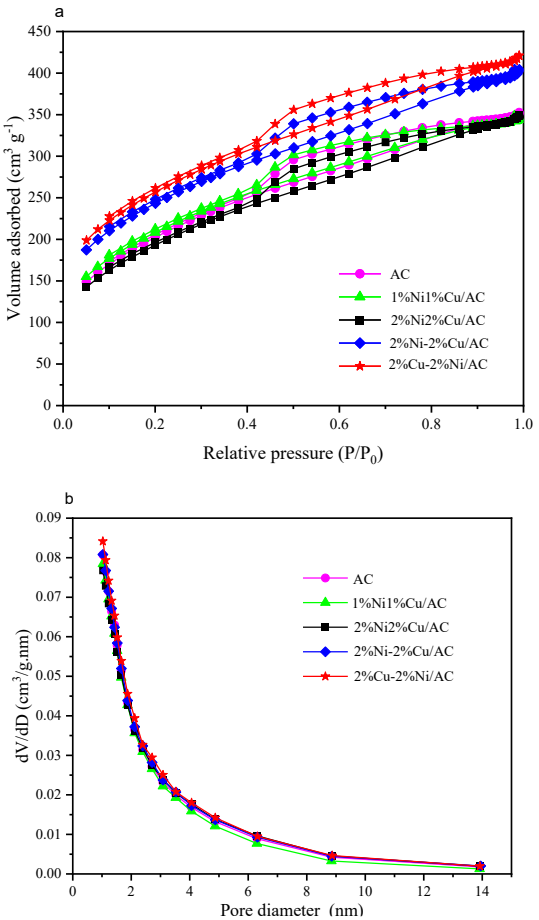

Fig. 6. (a) N_2 adsorption-desorption isotherm and (b) pore size distributions of AC and synthesized catalysts

In Fig. 6(a) the isotherm graph of AC and bimetallic catalysts shows a type I which is a characteristic of microporous material where the pore size is wider micropore material where the pore size includes wider micropores and possibly narrow mesopore <2.5 nm [41]. All samples have a type of hysteresis loop H4 and narrow slit-shaped pores and usually appear in materials that have combination of micro and mesopores [29]. This is also confirmed by the data in Table 2 where the average pore diameter is around 2.44 nm (categorized as mesopores but very close to micropores). In addition, in Fig. 6(b) shows the distribution of pore diameters in the range of 1 nm to 14 nm and dominated by size of 1-4 nm.

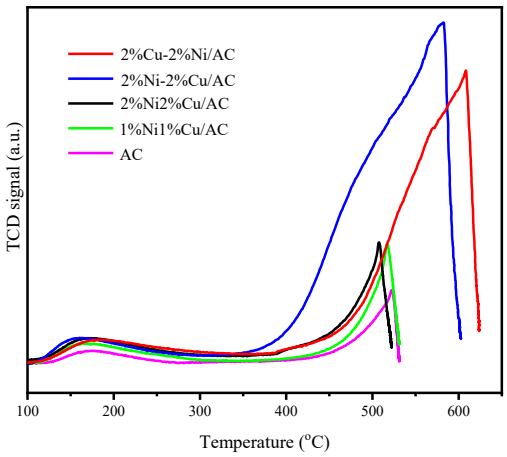

Fig. 7. NH_3-TPD analysis curve of AC and synthesized catalysts

The synthesized catalysts exhibit two desorption peaks as showed in Fig. 7. Desorption peak at 100-300 ˚C indicates the presence of weak acid site and >400 ˚C are the strong acid site. The results of the acidity values of all catalyst samples are presented in Table 2 and show that AC has the lowest total acidity. After the impregnation of Ni and Cu bimetals, an increase in acidity was observed. For catalysts with simultaneous impregnation, the more metal impregnated on AC, the higher its total acidity. This result confirmed with the EDX analysis, where 2%Ni2%Cu/AC has a higher impregnated Ni and Cu metal content compared to 1%Ni1%Cu/AC.

Based on the metal loading sequence with the same metal concentration, the order of acidity from highest to lowest is Ni2%-Cu2%/AC > Cu2%-Ni2%/AC > 2%Ni2%Cu/AC. The catalyst with metals impregnated simultaneously has lower acidity, likely due to the agglomeration of Ni and Cu metals in the 2%Ni2%Cu/AC catalyst, which reduces the distribution of metals on the AC surface. The agglomeration causes some active sites, which contribute to the catalyst's acidity, to not form properly or to be covered by aggregated metal particles.

3.2. Catalytic activity test

Table 3. Metal content of AC and synthesized catalysts

Catalysts	DBT Removal (%)
AC	73.12
1%Ni1%Cu/AC	79.87
2%Ni2%Cu/AC	82.76
2%Ni-2%Cu/AC	85.93
2%Cu-2%Ni/AC	84.60

In Table 3, it showed that the metal impregnation on the surface of AC enhances the catalytic ability to reduce DBT concentration. The increase in the amount of metal loaded on

the catalyst is also proportional to improvement in the catalysts effectiveness in the ODS-DBT process. Overall, the bimetallic catalysts impregnated sequentially as 2%Ni-2%Cu/AC and 2%Cu-2%Ni/AC exhibit higher catalytic activity compared to the simultaneous impregnation with the same metal concentration. This is related to the larger surface area as seen in Table 2, where pore blockages caused the surface area to decrease [37] while surface roughening and even metal distribution contribute to extra active sites [38] and higher total acidity compared to the 2%Ni2%Cu/AC. The 2%Ni-2%Cu/AC is the most effective in reducing DBT concentration in this study, achieving reduction of 85.93% due to higher acidity as seen in Table 2.

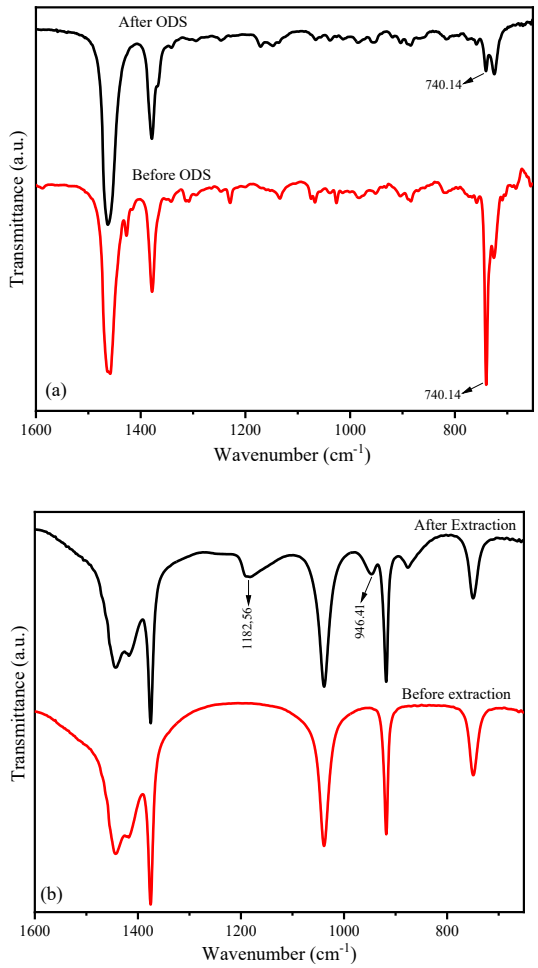

Fig. 8. FTIR spectra of (a) model fuel and (b) Acetonitrile before and after ODS

To confirm the success of the oxidation process of the model fuel and the extraction phase, FTIR analysis was conducted before and after the ODS process. After ODS the absorption peak at 740.14 cm^{-1}, which is a characteristic peak for DBT [42], showed a significant decrease in intensity seen in Fig. 8. In the spectrum of the acetonitrile phase after extraction, a new absorption peak at 946.41 cm^{-1} and 1182.56 cm^{-1} identified as the asymmetric stretching vibration modes of sulfoxide [43] and the presence of the -SO_2 group from sulfone [44,45].

3.3. Reaction condition optimization

Table 4. DBT removal in ODS with various reaction conditions using 2%Ni-2%Cu/AC catalyst

Reaction Condition				DBT Removal (%)
Catalyst Loading (g)	Reaction Time (min)	Temperature (˚C)	H_2O_2 Volume (mL)	
0.05	60	60	0.130	78.07
0.10	60	60	0.130	77.65
0.15	60	60	0.130	84.28
0.20	60	60	0.130	87.29
0.25	60	60	0.130	83.62
0.20	**20**	60	0.130	84.50
0.20	**40**	60	0.130	85.80
0.20	**60**	60	0.130	87.29
0.20	**90**	60	0.130	81.28
0.20	**120**	60	0.130	79.77
0.20	60	**30**	0.130	85.48
0.20	60	**40**	0.130	88.56
0.20	60	**50**	0.130	87.29
0.20	60	**60**	0.130	79.82
0.20	60	**70**	0.130	73.08
0.20	60	40	**0.066**	89.76
0.20	60	40	**0.130**	88.56
0.20	60	40	**0.260**	88.23
0.20	60	40	**0.390**	87.54
0.20	60	40	**0.660**	86.40

Table 4 shows the influence of catalyst loading on the percentage of DBT removal from the model fuel at 60°C over a duration of 1 hour. Different amounts of the catalyst from 0.05 to 0.25 g are evaluated in the increase of catalyst dosage provide more active sites and facilitating the oxidation process of DBT by H_2O_2 [8,46]. As the catalyst weight increased from 0.05 to 0.2 grams, the DBT conversion also rose. The increased amount of catalyst provided more active sites, facilitating the oxidation process of DBT by H_2O_2 [8,47]. A catalyst weight of 0.2 grams was the most effective in reducing DBT concentration as it offered optimal activity to accelerate the oxidation reaction. However, increasing the catalyst mass from 0.2 to 0.25 grams resulted in a slight decrease in DBT conversion, which was likely attributed to the aggregation of catalyst particles. This aggregation could block and obscure the active sites on the catalyst, thereby reducing the number of active sites available for the reaction [48]. Meanwhile, catalyst weights below 0.2 grams, although sufficient to initiate the DBT oxidation reaction, resulted in a slower reaction rate compared to using 0.2 grams of catalyst.

Variations in reaction time in the range of 20–120 min, under a temperature of 60 ˚C, oxidant to sulfur molar ratio (O/S) 10 and a catalyst weight of 0.2 g, were used to determine the optimum reaction time on the ODS-DBT. Table 4 shows that as the reaction time increases from 20 to 60 minutes, the conversion of DBT also increases. According to Yaseen et al. [14], a longer reaction time provides a greater opportunity for collisions between the reacting species and the active species of the catalyst, resulting in a higher reduction in DBT concentration. The highest reduction in DBT concentration

occurs at 60 minutes, reaching 87.26%, after that the percentage of DBT concentration reduction decreases. This decrease in DBT conversion can be attributed to the achievement of equilibrium, where all active sites of the catalyst have been utilized to oxidize DBT, thereby reducing the possibility of DBT oxidation on the catalyst surface.

DBT removal increase with increasing reaction temperature from 30 to 40 °C as seen in Table 4. This shows the endothermic nature of the ODS reaction of DBT. The increase in DBT conversion could be ascribed to the increase in the number of effective collisions between reactants and active sites on the catalyst surface. Increasing the temperature from 40 to 70°C resulted in a decrease in DBT conversion to 73.03%. Increasing the temperature can accelerate the desulfurization rate, but at higher temperatures it can increase the rate of thermal decomposition of H_2O_2 and have a negative impact on the performance of the catalyst.

$$C_{12}H_8S + 2H_2O_2 \rightarrow C_{12}H_8SO_2 + 2H_2O \quad (2)$$

The effect of O/S ratio was studied by varying the amount of H_2O_2 with the constant variables of 20 mL DBT, catalyst dosage of 0.2 g, time of 60 min, and temperature 40°C. The equation 2 shows that two moles of H_2O_2 are needed to oxidize one mol of $C_{12}H_8S$. In this study, 20 mL of 1200 ppm $C_{12}H_8S$ was used, which is equivalent to 0.00013 mol, so 0.00023 mol of H_2O_2 is needed to oxidize $C_{12}H_8S$ to $C_{12}H_8SO_2$. This amount is equivalent to 0.026 mL of 30% H_2O_2. In this study, the amount of oxidant was optimized by varying the volume of H_2O_2 to 0.066, 0.13, 0.26, 0.40 and 0.66 mL with a constant amount of DBT. Table 4 showed that the highest DBT removal is at a volume of 0.066 mL, which is 89.74%. The more H_2O_2 added, the lower the DBT conversion. This is likely because the increase in H_2O_2 concentration also increases the concentration of water formed during H_2O_2 decomposition. The presence of water in the ODS-DBT system can reduce the reactivity of the catalyst where water or H_2O_2 in large amounts can compete with DBT to interact with active sites on the catalyst surface [49–52].

3.4. Reusability test

Table 5. 2%Ni-2%Cu/AC catalyst reusability test under optimum condition

Number of Run	DBT Removal (%)
1	90.81
2	82.25
3	78.27
4	77.55

The stability of 2%Ni-2%Cu/AC catalyst was investigated in ODS-DBT process under the optimum reaction condition. After the first reaction, the catalyst was washed with acetonitrile and dried in an oven at 100˚C until its weight was constant and again tested in the next cycle of ODS reaction. The results in Table 5 indicate that the percentage of DBT concentration reduction decreased along with the increasing number of catalyst reuses. After four cycles the efficiency of the 2%Ni-2%Cu/AC catalyst to reduce DBT concentration decreased from 90.79% to 77.51%. The decrease of 2%Ni-2%Cu/AC catalyst is likely due to the presence of residual DBT and oxidation products that are still attached to the catalyst surface even after washing with acetonitrile.

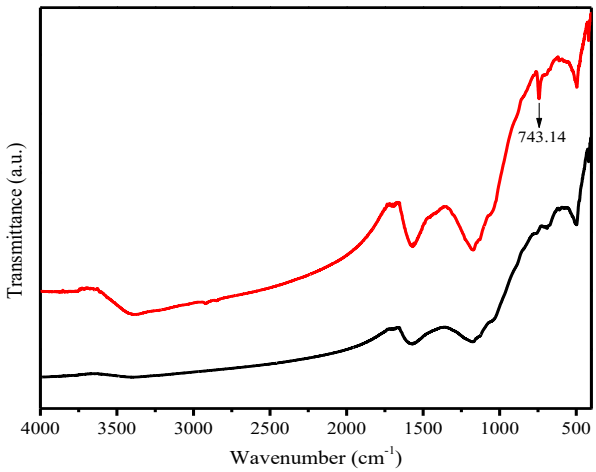

Fig. 8 FTIR Spectra of 2%Ni-2%Cu/AC after Reusability Test

The FTIR spectra of the catalyst after used in four cycles ODS in Fig 8. confirms the cause of the decrease in catalytic activity. This decrease can be caused by the presence of residual products or residual reactants that are still attached to the catalyst surface even after washing with Acetonitrile. This causes the adsorption process of reactants on the surface in the subsequent ODS process to be hampered so that the converted DBT becomes less. A new absorption peak appeared on the used catalyst at a wave number of 743.14 cm^{-1}, indicating the presence of DBT [42] on the catalyst surface.

3.5. Comparison with previous ODS-DBT studies

As shown in Table 6, although other studies have reported DBT removal rates exceeding 90%, these were typically achieved at lower DBT concentrations (600–800 ppm). In contrast, the 2%Ni–2%Cu/AC catalyst achieved 90.81% removal at a higher DBT concentration of 1200 ppm resulting in 109 mg of DBT removed per gram, demonstrating strong and efficient performance at milder and sustainable conditions that required a smaller catalyst dosage compared to Fe-promoted Co–Mo/Al_2O_3 and Ni–Mo/Al_2O_3 catalysts [53], and operated under milder conditions—including lower temperature, shorter reaction time, and reduced oxidant usage—than ZnO–AC and ZnO/γ-Al_2O_3 systems [7,54]. These advantages highlight the superior energy and material efficiency of the 2%Ni–2%Cu/AC catalyst with better performance. Furthermore, the use of activated carbon derived from bamboo waste enhances its sustainability, making it a promising candidate for industrial application, where reducing material input, energy consumption, and processing time contributes to more cost-effective and environmentally friendly production.

Table 6. Catalyst performance on ODS-DBT comparison with other studies

Catalyst	Feed	Reaction Condition	DBT removal per gram (mg/g)	Ref.
2%Ni-2%Cu/AC	20mL DBT (1200 ppm)	0.2 g catalyst weight, 60 minutes, 40 °C, and a H_2O_2 (30wt%) volume of 0.066 mL (7.5wt%)	109	This work
ZnO-AC	20mL DBT (500 ppm)	0.1 g catalyst weight, 120 minutes, 60 °C, and a H_2O_2 (30wt%) volume of 0.100 mL (11.25wt%)	93.8	[7]
Fe-Promoted Co-Mo/Al_2O_3 and Ni-Mo/Al_2O_3	10mL DBT (800 ppm)	0.4 g catalyst weight, 150 minutes, 60 °C, and 30wt% of H_2O_2	19.8	[53]
ZnO/γ-Al_2O_3	100 mL DBT (611 ppm)	100mL feed, 1 g catalyst weight, 80 minutes, 60 °C, and a H_2O_2 (1 M) volume of 4.0 mL	57.3	[54]

Note: DBT Removed (mg/g) = (ppm × feed volume in L) × (removal fraction): Catalyst weight

4. Conclusion

The impregnation of Ni and Cu bimetals onto activated carbon (AC) significantly enhanced the catalyst's acidity, with total acidity values increasing from 0.6215 mmol/g for bare AC to 0.8431 mmol/g and 0.9294 mmol/g for 1%Ni–1%Cu/AC and 2%Ni–2%Cu/AC, respectively. The method of metal impregnation played a crucial role in determining the physicochemical properties and catalytic performance. Among the catalysts tested, 2%Ni–2%Cu/AC prepared via sequential impregnation demonstrated the highest DBT removal efficiency (90.81%) under mild reaction conditions (0.2 g catalyst, 60 min, 40 °C, and 0.066 mL H_2O_2). This superior activity is attributed to stronger metal–support interactions, enhanced acidity, and more uniform metal dispersion. In contrast, simultaneous impregnation resulted in competition between Ni and Cu for active sites on the AC surface, leading to metal agglomeration and reduced catalytic performance. Overall, sequential metal impregnation proved to be a more effective strategy, offering improved surface characteristics and catalytic efficiency for oxidative desulfurization applications.

Acknowledgements

The authors would like to thank the Faculty of Mathematics and Natural Sciences, Gadjah Mada University, for supporting this research through the 2025 Flagship Research Grant Program(Grant No. 3968/UN1/FMIPA1.3/KP/PT.01.03/2025).

References

1. A.C. Tella, A.C. Oladipo, V.O. Adimula, O.A. Ameen, S.A. Bourne, and A.S. Ogunlaja, *Synthesis and crystal structures of a copper(ii) dinuclear complex and zinc(ii) coordination polymers as materials for efficient oxidative desulfurization of dibenzothiophene*, New J. Chem. 43 (2019) 14343–14354.
2. A. V. Akopyan, R.A. Mnatsakanyan, E.A. Eseva, D.A. Davtyan, P.D. Polikarpova, M.O. Lukashov, et al., *New Type of Catalyst for Efficient Aerobic Oxidative Desulfurization Based On Tungsten Carbide Synthesized by the Microwave Method*, ACS Omega 7 (2022) 11788–11798.
3. A. Rajendran, T.Y. Cui, H.X. Fan, Z.F. Yang, J. Feng, and W.Y. Li, *A comprehensive review on oxidative desulfurization catalysts targeting clean energy and environment*, J. Mater. Chem. A 8 (2020) 2246–2285.
4. M. Ahmadian, and M. Anbia, *Highly efficient oxidative desulfurization catalyzed by copper-based materials using hydrogen peroxide as oxidant*, Fuel 324 (2022) 124471.
5. B.S. Ahmed, L.O. Hamasalih, K.H. Hama Aziz, K.M. Omer, and I. Shafiq, *Oxidative Desulfurization of Real High-Sulfur Diesel Using Dicarboxylic Acid/H2O2 System*, Processes 10 (2022).
6. Y. Chen, Q. Tian, Y. Tian, J. Cui, and G. Wang, *Ultra-deep oxidative desulfurization of fuel with H2O2 catalyzed by mesoporous silica-supported molybdenum oxide modified by Ce*, Appl. Sci. 11 (2021) 1–15.
7. W. Trisunaryanti, S.D. Sumbogo, S.A. Novianti, D.A. Fatmawati, M. Ulfa, and Y.L. Nikmah, *ZnO-activated carbon blended as a catalyst for oxidative desulfurization of dibenzothiophene*, Bull. Chem. React. Eng. Catal. 16 (2021) 881–887.
8. S. Akbari Moghadam, G. Mazloom, A. Akbari, and F. Banisharif, *Supported vanadium oxide catalyst over HY-zeolite-alumina composite fabricated by extrusion for oxidative desulfurization of dibenzothiophene*, Mol. Catal. 532 (2022) 112731.
9. Y. Jia, G. Li, and G. Ning, *Efficient oxidative desulfurization (ODS) of model fuel with H 2O2 catalyzed by MoO3/γ-Al 2O3 under mild and solvent free conditions*, Fuel Process. Technol. 92 (2011) 106–111.
10. M. Ghahramaninezhad, and A. Ahmadpour, *A new simple protocol for the synthesis of nanohybrid catalyst for oxidative desulfurization of dibenzothiophene*, Environ. Sci. Pollut. Res. 27 (2020) 4104–4114.
11. J. He, Y. Wu, P. Wu, L. Lu, C. Deng, H. Ji, et al., *Synergistic Catalysis of the PtCu Alloy on Ultrathin BN Nanosheets for Accelerated Oxidative Desulfurization*, ACS Sustain. Chem. Eng. 8 (2020) 2032–2039.
12. A. Haruna, Z.M.A. Merican, and S.G. Musa, *Recent advances in catalytic oxidative desulfurization of fuel oil – A review*, J. Ind. Eng. Chem. 112 (2022) 20–36.
13. L. Chen, and Z.Y. Yuan, *Design strategies of supported metal-based catalysts for efficient oxidative desulfurization of fuel*, J. Ind. Eng. Chem. 108 (2022) 1–14.
14. M. Yaseen, S. Khattak, S. Ullah, F. Subhan, W. Ahmad, M. Shakir, et al., *Oxidative desulfurization of model and real petroleum distillates using Cu or Ni impregnated banana peels derived activated carbon–NaClO catalyst–oxidant system*, Chem. Eng. Res. Des. 179 (2022) 107–118.
15. M. Elena Manríquez-Ramírez, M.T. Valdez, L. V. Castro, M.E. Flores, and E. Ortiz-Islas, *Application of CeO2-V2O5 catalysts in the oxidative desulfurization of 4,6-dimethyl dibenzothiophene as a model reaction to remove sulfur from fuels*, Mater. Res. Bull. 153 (2022) 111864.
16. B. Fareed, F. Sher, F. Zafar, I. Ziani, B. Wang, R. Fatima, et al., *Advanced monometallic and bimetallic catalysts for energy efficient propylene production via propane dehydrogenation pathways–A review*, Appl. Energy 397 (2025).
17. L. Wang, N. Zuo, Z. Wang, D. Xie, Q. Liu, S. Li, et al., *Ultra-selective*

desulfurization of 4, 6-dimethyldibenzothiophene via carbon-sulfur bond cleavage with the bimetal single atom on N-rGO, J. Hazard. Mater. 399 (2020) 122803.

18. L. Marlinda, Rahmi, A. Aziz, A. Roesyadi, D.H. Prajitno, Y.W. Mirzayanti, et al., *Cobalt-nickel supported on desilicated HZSM-5 for the conversion of Reutealis trisperma (blanco) airy shaw oil to liquid hydrocarbon products*, Commun. Sci. Technol. 10 (2025) 87–97.
19. H.M. Kim, B.J. Kim, W.J. Jang, J.O. Shim, K.W. Jeon, H.S. Na, et al., *Effect of support materials and Ni loading on catalytic performance for carbon dioxide reforming of coke oven gas*, Int. J. Hydrogen Energy 44 (2019) 8233–8242.
20. E. Taer, L. Pratiwi, Apriwandi, W.S. Mustika, R. Taslim, and Agustino, *Three-dimensional pore structure of activated carbon monolithic derived from hierarchically bamboo stem for supercapacitor application*, Commun. Sci. Technol. 5 (2020) 22–30.
21. S.M.A. Mahanim, I. Wan Asma, J. Rafidah, E. Puad, and H. Shaharuddin, *Production of activated carbon from industrial bamboo wastes*, J. Trop. For. Sci. 23 (2011) 417–424.
22. W. Astuti, R.M. Ramadhan, and V.A. Octaviany, *Synthesis of Activated Carbon from Petung Bamboo Stems (Dendrocalamus Asper) Using Microwave-Assisted Pyrolysis (MAP) Process for Biogas Storage*, J. Bahan Alam Terbarukan 11 (2022) 58–67.
23. F. Visiamah, W. Trisunaryanti, and Triyono, *Microwave-assisted coconut wood carbon-based catalyst impregnated by Ni and/or Pt for bio-jet fuel range hydrocarbons production from Calophyllum inophyllum L. oil using modified-microwave reactor*, Case Stud. Chem. Environ. Eng. 9 (2024) 100722.
24. L. Romero-Castro, A.E. Galetti, M.S. Moreno, and M.N. Barroso, *Nanostructured Ni–Co catalysts: Effect of impregnation sequence and complexing agent*, Mater. Today Chem. 42 (2024) 102348.
25. N. Osakoo, R. Henkel, S. Loiha, F. Roessner, and J. Wittayakun, *Comparison of PdCo/SBA-15 prepared by co-impregnation and sequential impregnation for Fischer-Tropsch synthesis*, Catal. Commun. 66 (2015) 73–78.
26. I.S. Ismail, N.A. Rashidi, and S. Yusup, *Production and characterization of bamboo-based activated carbon through single-step H3PO4 activation for CO2 capture*, Environ. Sci. Pollut. Res. 29 (2022) 12434–12440.
27. Triyono, W. Trisunaryanti, J. Purbonegoro, and S.I. Aksanti, *Effect of cobalt impregnation methods on Parangtritis sand towards catalysts activity in hydrocracking of degummed low-quality Ujung Kulon Malapari oil into biohydrocarbons*, React. Kinet. Mech. Catal. (2023).
28. Q. Cai, Z. Fan, J. Chen, W. Guo, F. Ma, S. Sun, et al., *Dissolving process of bamboo powder analyzed by FT-IR spectroscopy*, J. Mol. Struct. 1171 (2018) 639–643.
29. A. Kamińska, J. Sreńscek-Nazzal, J. Serafin, P. Miądlicki, K. Kiełbasa, and A. Wróblewska, *Biomass-based activated carbons produced by chemical activation with H3PO4 as catalysts for the transformation of α-pinene to high-added chemicals*, Environ. Sci. Pollut. Res. 31 (2024) 40063–40082.
30. T.R. Brazil, M. Gonçalves, M.S.O. Junior, and M.C. Rezende, *Sustainable process to produce activated carbon from Kraft lignin impregnated with H3PO4 using microwave pyrolysis*, Biomass and Bioenergy 156 (2022) 106333.
31. G. Zeng, W. Li, S. Ci, J. Jia, and Z. Wen, *Highly Dispersed NiO Nanoparticles Decorating graphene Nanosheets for Non-enzymatic Glucose Sensor and Biofuel Cell*, Sci. Rep. 6 (2016) 1–8.
32. A. Chinthakuntla, K. Venkateswara Rao, C. Ashok, Kv. Rao, and C. Shilpa Chakra, *STRUCTURAL ANALYSIS OF CuO NANOMATERIALS PREPARED BY NOVEL MICROWAVE ASSISTED METHOD*, J. Atoms Mol. 4 (2014) 803–806.
33. P. López, G. Mondragón-Galicia, M.E. Espinosa-Pesqueira, D. Mendoza-Anaya, M.E. Fernández, A. Gómez-Cortés, et al., *Hydrogen production from oxidative steam reforming of methanol: Effect of the Cu and Ni impregnation on ZrO 2 and their molecular simulation studies*, Int. J. Hydrogen Energy 37 (2012) 9018–9027.
34. Z. Liang, G.P. Kovács, C. Gyuricza, and A. Neményi, *Potential use of bamboo in the phytoremediation in of heavy metals: A review*, Acta Agrar. Debreceniensis 2022 (2022) 91–97.
35. M.E.A. Montaño, L. Effting, C.L.B. Guedes, G.G.C. Arizaga, R.M. Giona, P.H.Y. Cordeiro, et al., *Performance assessment of activated carbon thermally modified with iron in the desulfurization of biogas in a static batch system supported by headspace gas chromatography*, J. Anal. Sci. Technol. 15 (2024).
36. I. Kurnia, S. Karnjanakom, I. Irkham, H. Haryono, Y.A. Situmorang, A. Indarto, et al., *Enhanced adsorption capacity of activated carbon over thermal oxidation treatment for methylene blue removal: kinetics, equilibrium, thermodynamic, and reusability studies*, RSC Adv. 13 (2022) 220–227.
37. E. Aryee, A.K. Dalai, and J. Adjaye, *Synthesis and Characterization of NiMo Catalysts Supported on Fine Carbon Particles for Hydrotreating: Effects of Metal Loadings in Catalyst Formulation*, Front. Chem. Eng. 3 (2021) 1–14.
38. R.S. Neisan, N.M.C. Saady, C. Bazan, S. Zendehboudi, and T.M. Albayati, *Adsorption of copper from water using TiO2-modified activated carbon derived from orange peels and date seeds: Response surface methodology optimization*, Heliyon 9 (2023) e21420.
39. T. Shoosri, P. Chotiwilaiwan, T. Rattanapornchaiwat, T. Teerawatananond, T. Miyake, J. Panpranot, et al., *Bimetallic copper- and nickel-rich Cu-Ni phyllosilicate catalysts for the liquid phase selective hydrogenation of furfural to furfuryl alcohol*, RSC Adv. 14 (2024) 38232–38244.
40. T. Vandevyvere, M.K. Sabbe, J.W. Thybaut, and J. Lauwaert, *Enhancing Stability of γ-Al2O3-Supported NiCu Catalysts by Impregnating Basic Oxides in the Hydrodeoxygenation of Anisole*, Catalysts 14 (2024) 1–16.
41. M. Thommes, K. Kaneko, A. V. Neimark, J.P. Olivier, F. Rodriguez-Reinoso, J. Rouquerol, et al., *Physisorption of gases, with special reference to the evaluation of surface area and pore size distribution (IUPAC Technical Report)*, Pure Appl. Chem. 87 (2015).
42. E. Syntyhaki, A. Detsi, and D. Karonis, *Assessment of the Oxidative Desulfurization of Middle Distillate Surrogate Fuels with Spectroscopic Techniques*, J. Anal. Methods Chem. 2020 (2020).
43. W. Trisunaryanti, S.A. Novianti, D.A. Fatmawati, T. Triyono, M. Ulfa, and D. Prasetyoko, *Simple and Green Preparation of ZnO Blended with Highly Magnetic Silica Sand from Parangtritis Beach as Catalyst for Oxidative Desulfurization of Dibenzothiophene*, Indones. J. Chem. 22 (2022) 455–467.
44. K. Castillo, J.G. Parsons, D. Chavez, and R.R. Chianelli, *Oxidation of dibenzothiophene to dibenzothiophene-sulfone using silica gel*, J. Catal. 268 (2009) 329–334.
45. K.C. Schreiber, *Infrared Spectra of Sulfones and Related Compounds*, Anal. Chem. 21 (1949) 1168–1172.
46. A. V. Akopyan, A.O. Shlenova, P.D. Polikarpova, and A. V. Vutolkina, *High-Performance Heterogeneous Oxidative Desulfurization Catalyst with Brønsted Acid Sites*, Pet. Chem. 62 (2022) 636–642.
47. M.E. Manríquez, A.L. Ortiz, M. Trejo-Valdez, L. V. Castro, and E. Ortiz-Islas, *Catalytic oxidative desulfurization of 4,6-dimethyl dibenzothiophene by phosphotungstic acid loaded on Al2O3, V2O5, and ZrO2 oxides*, React. Kinet. Mech. Catal. 135 (2022) 1523–1539.
48. A. Hesami, and S. Shahhosseini, *Optimization of a novel catalytic extractive oxidative process for desulfurization of model and real fuels using a metal-free heterogenous catalyst (B4C)*, Case Stud. Chem.

Environ. Eng. 9 (2024) 1–13.

49. C.M. Lousada, A.J. Johansson, T. Brinck, and M. Jonsson, *Mechanism of H 2O 2 decomposition on transition metal oxide surfaces*, J. Phys. Chem. C 116 (2012) 9533–9543.
50. G. Yu, D. Jin, F. Zhang, Q. Li, Z. Zhou, and Z. Ren, *Oxidation-extraction desulfurization of fuel with a novel green acidic deep eutectic solvent system*, Fuel 329 (2022) 125495.
51. N. Ahmad, E.S. Fitri, A. Wijaya, Amri, Mardiyanto, I. Royani, et al., *Catalytic Oxidative Desulfurization of Dibenzothiophene Utilizing Composite Based Zn/Al Layered Double Hydroxide*, Bull. Chem. React. Eng. Catal. 17 (2022) 733–742.
52. X. Zeng, A. Adesina, P. Li, H. Wang, and R. Zhou, *Enhanced adsorptive-oxidative desulfurization of dibenzothiophene over Ti-MWW using cumene hydroperoxide as oxidant*, Korean J. Chem. Eng. 39 (2022) 96–108.
53. Y. Muhammad, A. Shoukat, A.U. Rahman, H.U. Rashid, and W. Ahmad, *Oxidative desulfurization of dibenzothiophene over Fe promoted Co–Mo/Al2O3 and Ni–Mo/Al2O3 catalysts using hydrogen peroxide and formic acid as oxidants*, Chinese J. Chem. Eng. 26 (2018) 593–600.
54. A.A. Aabid, J.I. Humadi, G.S. Ahmed, A.T. Jarullah, M.A. Ahmed, and W.S. Abdullah, *Enhancement of Desulfurization Process for Light Gas Oil Using New Zinc Oxide Loaded Over Alumina Nanocatalyst*, Appl. Sci. Eng. Prog. 16 (2023) 6756.